EROSION OF ITER DIVERTOR ARMOUR AND CONTAMINATION OF SOL AFTER TRANSIENT EVENTS BY EROSION PRODUCTS

B.N. Bazylev, I.S. Landman, S.E. Pestchanyi

Forschungszentrum Karlsruhe (FZK), Institute for Pulsed Power and Microwave Technology, P. B. 3640, 76021 Karlsruhe, Germany

Plasma impact to the divertor expected in the tokamak ITER during ELMs or disruptions can result in a significant surface damage to CFC- and tungsten armours (brittle destruction and melting respectively) as well as in contamination of SOL by evaporated impurities. Numerical investigations for tungsten and CFC targets provide important details of the material erosion process. The simulations carried out in FZK on the material damage, carbon plasma expansion and the radiation fluxes from the carbon impurity are surveyed.
PACS: 52.40Hf

1. INTRODUCTION

In the future tokamak ITER the high power transient processes such as bursts of edge localized modes (ELMs) that accompany with the frequency of 1-10^2 Hz the normal tokamak operation and the disruptions that sometimes interrupt the quasi-stationary discharge, will be probably much more serious problem than in the available tokamaks. This is due, for instance, to large plasma energy up to 0.5 GJ assumed in ITER, which is of two orders larger than in now available tokamaks. The heat deposition Q in the range about $0.5 - 3$ MJ/m^2 on the time scale τ about $0.1 - 1$ ms for ELMs and $Q \sim 10 - 30$ MJ/m^2 at $\tau \sim 1 - 10$ ms for the disruptions are expected at the divertor surface [1]. The plasma facing components (PFC) of the ITER divertor are going to be made of carbon fibre composites (CFC) in the most loaded part at the separatrix strike position (SSP) and of tungsten (W-brushe) in the other parts. The large loads can cause surface erosion of the armour and evaporation of a thin layer of the material that after ionization in the impacting plasma stream acts as a plasma shield which simultaneously propagates in the scrape-off layer (SOL).

The erosion of the armour materials and the contamination of the confined plasma have to be estimated before ITER itself faces the plasma wall interaction problems. As the expected fluxes are not achievable at present tokamaks, it follows that the behaviour of the involved materials and the impurity plasma dynamics must be simulated numerically. However, the only way to obtain confidence of the used assumptions and theoretical models is a validation of the modelling by experiments, because in reality unexpected physical processes might play an important role. Therefore non-tokamak validation experiments are necessary.

This work surveys latter theoretical investigations carried out in FZK for the divertor armour damages and the impurity propagation in SOL applying and upgrading earlier developed codes. The computational tool applied for direct calculation of wall loads and plasma processes is two-dimensional (2D) RMHD (radiation-magneto-hydrodynamics) code FOREV−2D [2]. ITER relevant simulations with it for SOL are described in section 2. For simulation of the damage to tungsten surfaces the incompressible fluid dynamics code MEMOS-1.5D [3] is applied. The validation of the code against experiments on the plasma guns [4-6] is explained. The simulations with MEMOS-1.5D are presented in sect. 3. For PFC made of carbon-based materials the main erosion effect under the high heat fluxes is brittle destruction. In this case the thermomechanics code PEGASUS-3D [7] was applied. The brittle destruction simulations are described in sect. 4.

2. PLASMA PROCESSES IN SOL

The code FOREV-2D models the hot deuterium-tritium-helium plasma lost across the separatrix into SOL during a transient event, its propagation towards the wall and impact on the armour surface. It calculates also a self-consistent evaporation, ionization of carbon-, tungsten- and beryllium atoms, the radiation transport in the contaminated plasma and backward propagation of the erosion products into SOL. The code was created aiming simulations for a dense plasma shield in front of the surface at the disruption armour loads. Therefore the algorithm described slab geometry and one-fluid plasma, which was sufficient at the density above 10^{21} m^{-3} [2]. Since the reference regime of ITER operation will be probably the ELMy H-mode, recently FOREV-2D was upgraded for adequate tokamak relevant simulations at lower heat fluxes when the vapour shield is rather weak or absent. Now FOREV-2D models the whole SOL, the x−point and inner- and outer divertor plates. The ion fluids of D, T, He, He$^+$ and all charge states of C are simultaneously simulated. The code calculates also the quite important radiation transport in the carbon emission lines, accounting for reabsorption of line radiation.

In the ELM scenario the hot plasma losses from the pedestal region through the separatrix with a velocity

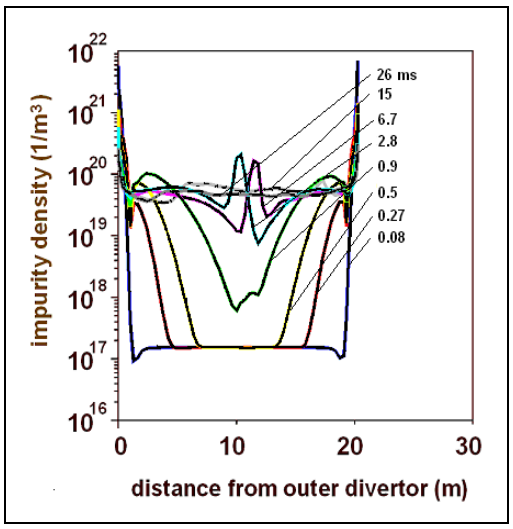

Fig. 1. Carbon plasma density profiles along the tokamak separatrix at different time moments

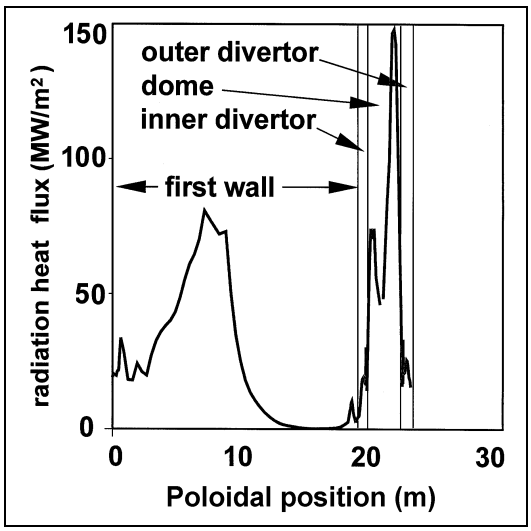

Fig. 2. Radiation load onto ITER vessel walls calculated with FOREV

determined by a specified Q and τ. It is assumed that the lost plasma appears then in SOL having an exponential density profile with maximum density n at the separatrix. In different simulations the values of n were varied in the range $2–7\times10^{19}$ m^{-3}, initial plasma temperature from 1 to 3 keV, and τ in the range 0.1–0.5 ms. The hot plasma propagates towards the CFC divertor armour legs, heats them and causes vaporization at their surfaces. The carbon vapour propagates backwards finally filling the whole SOL.

As an example, Fig. 1 demonstrates the profiles of carbon plasma density and temperature at several time moments t after the start of ELM at $t = 0$. Plasma streams have expanded from the inner- and outer divertor legs and then collided at ~3 ms. The density peak after this collision exists until 7 ms. This simulation corresponds to $Q = 0.8$ MJ/m^2 and $\tau = 0.3$ ms. The vaporisation starts at around 20-25 μs approximately at the same time on the inner- and outer divertor plates.

Typical radiation flux distribution calculated at the first wall at $t = 15$ ms is shown in Fig. 2. At this moment the carbon plasma is distributed almost uniformly along the separatrix in SOL and in the divertor legs. The maximal radiation heat load is on the dome and adjoining parts of divertor most filled with the radiative impurity. A smaller peak of the radiation flux is seen at the top of the main chamber, where the plasma thickness increased due to a divergence of the poloidal magnetic field.

3. BEHAVIOUR OF MOLTEN TUNSTEN

3.1. ITER relevant simulations

The erosion of a metallic surface under the loads exceeding the melting threshold is caused substantially by the melt motion. The melt motion develops mainly due to the variations of plasma pressure across the divertor plate of a width of 0.2 m. For ITER, the maximum pressure at the surface during a disruption can be of the order of 1 bar and during an ELM of 0.1 – 0.2 bar.

The simulations for tungsten armour under the disruptions loads are described in [3] where a large crater depth of a few tenth of μm was obtained. Now the regimes typical of the type I ELM are discussed following [8]. ITER operation in the H-mode is the regime with multiple ELMs. The ELM energy can exceed the melting threshold. After a single ELM, melt motion produces surface roughness of a rather small magnitude, which is nevertheless significantly larger than the thickness of vaporized surface layer (the evaporation thickness). However, during each ITER discharge more than 10^3 ELMs are expected. From one hand, the total roughness may accumulate and become rather large. From the other hand, during ELMs the separatrix strike position (SSP) moves rather unpredictably across the armour plate [9] which can average the roughness.

Tungsten target damage for the ITER discharges interspaced by ELMs has been simulated with the code MEMOS–1.5D which describes surface melting in the 'shallow water' approximation [10]. The melt motion is modelled taking into account the surface tension, viscosity of molten metal and the radiative losses from the hot tungsten surface. The plasma pressure gradient across the divertor plate, the gradient of surface tension and the Lorentz force of the currents crossing the melt layer immersed in the strong magnetic field produce the melt acceleration. During each ELM the SSP was assumed motionless but stochastically changing across the plate from ELM to ELM, obeying the Gaussian distribution. In the coordinate frame of the random SSP, the time dependent spatial profiles of heat fluxes and plasma pressure at the target surface were calculated with FOREV–2D taking into account the plasma shield effect.

The simulations demonstrated that one single ELM of $\tau = 0.3$ ms with Q varying from 1 to 2 MJ/m^2 produces

melting without evaporation. At $Q > 2.5$ MJ/m^2 the vapour shield forms significantly so that the pressure

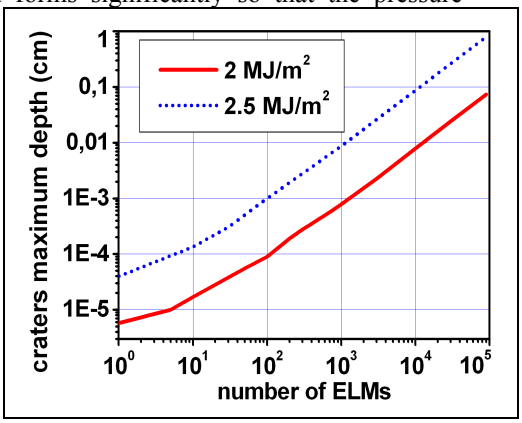

Fig. 3. The dependence of crater depth on the number of ELMs for $\delta = 0.1$ m obtained with MEMOS–1.5D

gradient becomes essential. In the regimes with the melt motion, the magnitude of surface roughness varies in range of 0.3 – 0.5 μm, the melt velocity V is of 0.5 m/s, and the evaporation thickness per single ELM of 0.1 μm.

For multiple ELMs, the Gaussian distribution of SSP with the dispersion $\delta = 0.1$ m results in a significant decrease of the crater depth compared to the case with fixed SSP. It is concluded that in the case of the stochastic SSP the evaporation mechanism becomes the main reason of erosion at the ELM number larger than 10^3, and thus the erosion rate acquires a linear dependence on the number of ELMs. For $Q < 1 – 2$ MJ/m^2 the number of ELMs to erode 1 cm of tungsten armour is obtained to be about $10^5 – 10^6$ (see Fig. 3)

3.2 Validations of MEMOS-1.5D

The tokamak simulators used for validation of the MEMOS-1.5D so far are the electron beam test facilities JUDITH [11] and JEBIS [12] and also the plasma guns MK –200UG [4], QSPA-Kh50 [5] and QSPA–T [6]. The code was earlier validated comparing numerical results with JUDITH for beryllium and JEBIS for tungsten [3]. As a tokamak simulator, each facility has advantages and disadvantages. Plasma itself, as a natural substance for the required loads, presents the main advantage of the plasma guns. Their main drawback is short pulse durations (not more than 0.5 ms). The electron beam high heat fluxes can last much longer time covering the required time scales but the beam pressure is negligibly low, which hampers the application of e-beams to metallic targets.

Earlier attempts to validate MEMOS-1.5D by the plasma gun MK-200UG failed. In the calculations with the load pulses of MK-200UG of 0.05 ms a negligible damage has been obtained in the simulations, in contrast to the experiments. Nevertheless, the calculations discovered that if the load would last longer, even as an energetic tail of a small magnitude, the melt motion would get substantial due to a non-zero melt velocity. Even without the energetic tail the calculated resolidification time was obtained to be much larger (of 0.35 ms) than the impact duration. The importance of

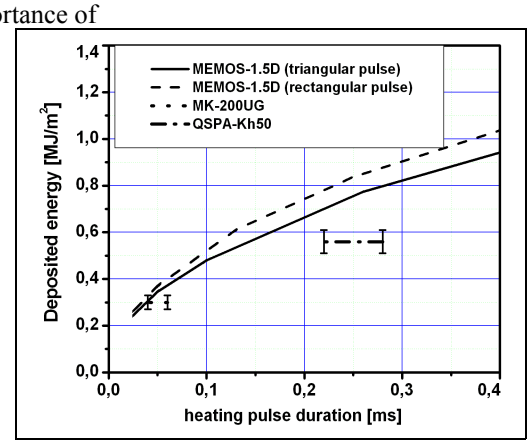

Fig. 4. Comparison of experimental- and numerical tungsten melting threshold

measurements on a longer time scale has been recognized. Finally in an experiment with copper target a high surface temperature keeping for at least 0.7 ms was obtained, which converged theoretical and experimental results.

Other validations of MEMOS-1.5D concerned the tungsten melting threshold. At such low load regime the energetic tail of MK-200UG is not important. The tungsten surface temperature T_w was measured for varied Q. During the exposition T_w first reaches T_{melt} at Q of 0.28 MJ/m^2, and T_w remains less than T_{melt} at lower Q. At Q of 0.4 MJ/m^2, T_w fast increases up to T_{melt} but then it remains at this value: evidently the absorbed energy flux is consumed for melting. After these measurements it was concluded that tungsten melting starts at $Q \approx 0.30$ MJ/m^2, which is considered as the melting threshold.

Calorimetric measurements of Q at the facility QSPA-Kh50.for multiple (up to 300) pulse irradiations of $\tau = 0.25$ ms provided the determination of the melting threshold. After initial exposures the melting threshold was determined as 0.56 MJ/m^2. However, after 150 exposures the melting threshold decreased to 0.45 MJ/m^2, which seems due to material modification and the development of the bulk cracks parallel to the target surface that cause decrease of thermal conductivity in a pre-surface layer.

For checking the experimental results obtained at MK-200UG and QSPA-Kh50 and aiming MEMOS validation, the tungsten melting threshold was also calculated. In the calculations the triangle and rectangular shapes of the impinging plasma load in time are assumed, with the pulse durations covering the range 0.05-0.25 ms. Fig. 4 illustrates the experimental results mentioned and the numerical results obtained with MEMOS: they are in a reasonable agreement.

4. BRITTLE DESTRUCTION OF CFC

The complicated structure of CFC is modelled in terms of involved properties: the thermal conductivity, the

coefficient of thermal expansion and the Young's modulus. A complicated three-dimensional structure of

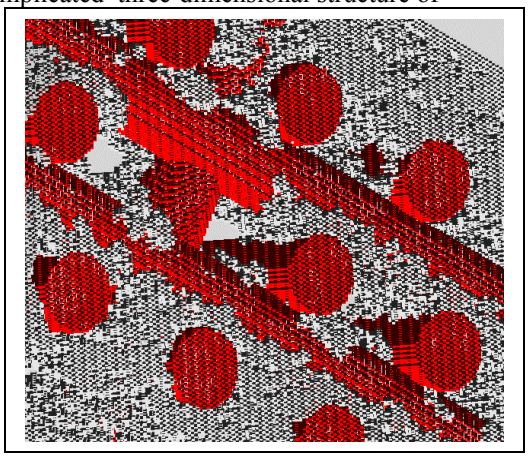

Fig. 5. Destruction of CFC obtained in the PEGASUS-3D simulation

different sorts of graphite constitutes CFC. It includes a framework consisting of bunches of fibres, so called tows [13], and a matrix that fills the space between the tows. CFC has good thermomechanical properties at surface temperatures at least up to 1.5×10^3 K, for instance a large thermal conductivity χ, in the fibres up to 10^3 W/mK. However, in average χ is strongly anisotropic and varies from 10^2 to 3×10^2 W/mK [14].

At the transient events the behaviour of CFC becomes problematic. For instance, CFC samples after irradiation by the plasma pulses of $Q = 10$ MJ/m^2 at $\tau \sim 0.05$ ms at MK–200UG and QSPA–T showed a drastic surface destruction with deep caverns of several hundred of μm and a strong damage along the longitudinal tows [15].

For analyses of the properties of CFC at the high heat fluxes the code PEGASUS–3D was applied [16]. The matrix and the tows are described by means of several millions of numerical cells of one-micrometer size. Some grains built of different groups of the cells simulate the graphite structure. Neighbour grains contact by means of mechanical- and heat conduction bonds.

In the simulations, the following typical parameters along and across the fibres are used: -1.5×10^{-6} and 20×10^{-6} K^{-1} for the thermal expansion coefficient, 500 and 20 GPa for the Young's modulus, 10^3 and 10^2 W/mK for the thermal conductivity, respectively.

A new mechanism of macroscopic erosion was discovered and named the local overheating erosion. Large local thermostress reaching a failure threshold removes the bond between the grains, thus producing a crack. The crack interrupts the local heat conduction. To maintain the given heat flux the temperature gradient becomes locally larger, increasing stress in the vicinity of the crack and producing new cracks. At the disruptive scale of the load, it is found that the cracks are mainly concentrated in the matrix around the tows. At the surface, the cracked out matrix particles are assumed to emit. Horizontal tows under the removed matrix and the caverns at the eroded surface appear, as it is shown in

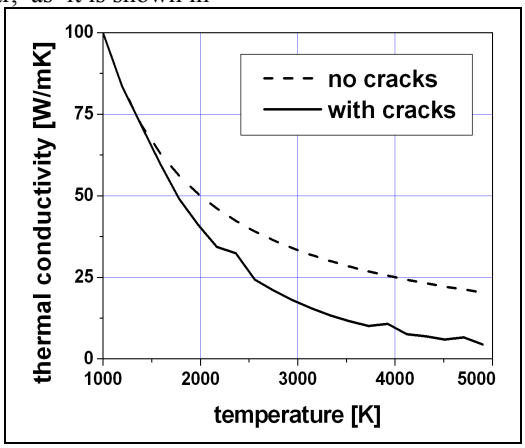

Fig. 6. Thermal conductivity of CFC matrix with- and without cracking obtained in the simulation

Fig. 5, which is rather similar to the experiments [15].

The thermostress due to anisotropy of thermal expansion coefficient and the Young's modulus of CFC was obtained in PEGASUS-3D simulations to be much larger than the thermostress due to the temperature gradient. This result leaded to a new approach for description of thermal transport in CFC [17]. The local crack density N is assumed to depend on T only and the dependence on ∇T is neglected: $N = N(T)$. From this approximation follows that an average function of effective macroscopic thermal conductivity $\kappa(T)$ exists that accounts for $N(T)$, which enabled to simplify heat transport modelling in cracked graphite materials. Fig. 6 demonstrates the influence of cracking on the typical thermal conductivity of CFC matrix obtained in the calculation.

5. SUMMARY

The described investigations are published and presented elsewhere (Refs. [2,3,7,8,16-19]). The main achievements and problems are as follows.

In the radiation transport calculations for carbon impurity, the line radiation dominates. It is to note that the data for line shapes need improvements, which demands significant effort for producing new opacities.

The stochastic distribution of SSP in MEMOS-1.5D reduces tungsten target erosion because of smoothing the surface roughness caused by the melt motion at each single ELM. Validation of MEMOS against plasma gun experiments at the tungsten melting threshold was successful. The tungsten melting threshold obtained in the experiments is in a reasonable agreement with the calculations of MEMOS, which justifies the application of the code for investigation of melt motion damage at the tokamak conditions.

The physical picture for CFC needs further development. PEGASUS-3D has to be validated against averaged thermophysical properties of CFC. From

comparison of the simulations and the experimental observations it is concluded that the experiments confirm the simulation concerning the development of the caverns and cracking horizontal tows.

REFERENCES

[1] Federici et al. // *Journ. Nucl. Mat*. (*11).*2003, p.313-316.
[2] H. Wuerz et al. // *Fus. Sci. Techn*. (*40)*. 2001, p. 191.
[3] B. Bazylev, H.Wuerz. // *Journ. Nucl. Mater.* (*69).* 2002, p. 307-311.
[4] N.I. Arkhipov et al. // *J. Nucl. Mater.* (*767).*1996, p.233-237.
[5] V.I. Tereshin et al. // *J. Nucl. Mater.* (*686).* 2003, p.313-316.
[6] V. Belan et al. // *Proc. 20th SOFT Marseille, France, 7-11 Sept. 1998.* v.1, p. 101
[7] S.E. Pestchanyi, H. Wuerz. // *Fus. Eng. Design*. 66-68C, 271, 2003.
[8] B. Bazylev et al. Erosion of divertor tungsten armour after many ELMs. // *Proc. 30th EPS Conf. on Contr. Fus. And Plasma Phys., St. Petersburg, Russia, 7-11 July 2003* // ECA v. 27A, P-2.44
[9] J. Lingertat et al. // *J.Nucl.Mater*. (*402*).1997,p.241-243.
[10] L.D. Landau, E.M. Lifshits. Course of theoretical physics. // *Fluid mechanics*, Oxford u.a.: Butterworth-Heinemann, 2000, V.6
[11] J.Linke et al. // *J.Nucl.Mater*. 290-293, 1102 (2001)
[12] K. Nakamura et al. , Fus. Eng. Des., 39-40 (1998) 285
[13] H. O. Pierson. "Handbook of carbon, graphite, diamond and fullerenes". (Noyes publications, New Jersey, 1993) p. 189
[14] J.P. Bonal, D. Moulinier. Thermal properties of advanced carbon fiber composites for fusion application. Rapport DMT/95-495. CEA. Direction des reacteurs nucleaires. Departement de mecanique et de technologie (1995)
[15] N.I. Arkhipov et al. Journ. Nucl. Mater. 307-311 (2002) 1364
[16] S.E. Pestchanyi et al., Estimation of carbon fibre composites as ITER divertor material. The paper will be published in Journ. Nucl. Mater. in 2004
[17] S.E. Pestchanyi, I.S. Landman, Physica Scripta, T111 (2004) 218
[18] I.S. Landman et al., Physica Scripta, T111 (2004) 206
[19] I.S. Landman et al., Simulation of tokamak armour erosion and plasma contamination at intense transient heat fluxes in ITER. A report at the Int. Conf. Plasma Surface Interactions, Portland Main, U.S.A., May 24-28, 2004

ЭРОЗИЯ ДИВЕРТОРНЫХ ПЛАСТИН В ТОКАМАКЕ ИТЕР И ЗАГРЯЗНЕНИЕ ПЛАЗМЕННОГО СКИН-СЛОЯ ПРОДУКТАМИ ЭРОЗИИ

Б.Н. Базилев, И.С. Ландман, С.Е. Песчаный

Воздействие плазмы на дивертор, предполагаемое в ИТЕР при развитии ЭЛМ неустойчивостей в скин-слое или при срывах, может вызвать как значительное поверхностное повреждение (хрупкое разрушение и плавление соответственно) диверторных пластин, изготовленных из графитовых композитов и вольфрама, так и загрязнение скин-слоя испарившимися примесями. Численные расчеты с вольфрамовыми и композитными мишенями проясняют важные детали процесса эрозии материалов. Дан обзор расчетов, проводимых в НЦК, по повреждению материалов, распространению углеродной плазмы и излучению углеродной примеси.

ЕРОЗІЯ ДИВЕРТОРНЫХ ПЛАСТИН У ТОКАМАКЕ ИТЕР І ЗАБРУДНЕННЯ ПЛАЗМЕННОГО СКИН-ШАРУ ПРОДУКТАМИ ЕРОЗІЇ

Б.Н. Базилєв, І.С. Ландман, С.Є. Піщаний

Вплив плазми на дивертор, передбачуваний в ИТЕРі при розвитку ЕЛМ нестійкостей у скін-шарі або при зривах, може викликати як значне поверхневе ушкодження (тендітне руйнування і плавлення відповідно) диверторних пластин, виготовлених із графітових композитів і вольфраму, так і забруднення скін-шару домішками, що випарувалися. Чисельні розрахунки з вольфрамовими і композитними мішенями проясняють важливі деталі процесу ерозії матеріалів. Дано огляд розрахунків, проведених у НЦК, по ушкодженню матеріалів, поширенню вуглецевої плазми і випромінюванню вуглецевої домішки.